Fault tolerant control based on continuous twisting algorithms of a 3-DoF helicopter prototype

Fault Tolerant Control based on Continuous Twisting Algorithms of a 3-DoF Helicopter Prototype

U. Pérez-Ventura[a], E. Capello[b,c], E. Punta[c], L. Fridman[a,*]

[a] *National Autonomous University of Mexico, Department of Control and Robotics, Division of Electrical Engineering, Engineering Faculty, C.P. 04510, Mexico city, Mexico*
[b] *Department of Mechanical and Aerospace Engineering, Politecnico di Torino, Corso Duca degli Abruzzi 24, 10129 Torino, Italy*
[c] *Institute of Electronics, Computer and Telecommunication Engineering, National Research Council of Italy (CNR-IEIIT) Politecnico di Torino, Corso Duca degli Abruzzi 24, 10129 Torino, Italy*

Abstract

Fault tolerant controllers based on the Continuous Twisting Algorithm (CTA) of order two and three are designed for a three-degree-of-freedom (3-DoF) helicopter prototype. Detection and isolation of actuator's faults (DC motors) are carried out by means of residual-based equations and exploiting a third-order sliding mode differentiator. Moreover, intermittent and persistent faults in the actuation system are induced by software to verify the effectiveness of the proposed procedure, which detects and isolates these failures. A comparison with respect to a classic observer-based FDI procedure is given to highlight the performance of the proposed method. Finally, simulations and real-time experiments confirm that CTA-based controllers counteract additive faults. Filtering signals obtained by residual equations is suggested in order to mitigate the effects of noises and fast-parasitic dynamics on the FDI procedure.

Keywords: Fault detection and isolation; Fault tolerant control; Sliding-mode control.

*Corresponding author
Email address: lfridman8@unam.mx (L. Fridman)

1. Introduction

In the last decade, for improving the safety of industrial and mechanical process, researchers focused the attention on fault tolerant controllers (FTCs). The main objective of this paper is to provide a *robust* controller, able to mitigate consequences of faults in the actuators of a 3-DoF helicopter prototype, manufactured by the Quanser Company [1]. As well known, sliding-mode controllers (SMCs) drive the system trajectories to the equilibrium point even in presence of matched perturbations [2]. Robust stabilization of the helicopter dynamics were provided via *discontinuous* sliding-mode controllers in [3, 4, 5]. However, discontinuous inputs deteriorate the DC motors and power supplies used for control of the 3-DoF helicopter prototype.

Continuous sliding mode controllers were implemented in the 3-DoF helicopter prototype to avoid the problems of discontinuous control signals mentioned above. In [6], an adaptive Super-Twisting controller with growing gains was used to mitigate the perturbations in simulations and real-time experiments. However, bi

when the perturbations are decreasing the controller gains are keeping big values, causing high energy consumption due to the presence of unmodeled dynamics, [7]. Robust tracking via continuous sliding-mode controllers was achieved with real-time experiments in [8, 9]. However, taking into account second-order sliding mode controllers, they can not ensure the best possible tracking and estimation accuracy, [10].

As proposed in [11], FDI techniques can be divided in three categories: (i) knowledge-based approach, (ii) signal processing-based approach, and (iii) analytical model-based approach. The first of these techniques strongly depends on the experience of the control operator. For example, the expert system can use a combination of object-oriented modeling [12] or logic-based approach as in [13]. The second approach is based on the idea of hardware redundancy, this means that several sensors measuring the same data are installed on-board to characterize the faults, as usually done off-line in power systems for instance.

Drawbacks of this approach are related to need of several measurements without ensuring real-time detection of faults in some cases. To obtain measurement redundancy, extra sensors are required but this causes an increase of the system cost. The model-based methods of fault detection were developed by using input and output signals and applying dynamic process models [14, 15]. The interest on this third approach is increased in the last years due to the improvement on modeling techniques [16]. In details, as presented in [17], these methods are based, e.g., on parameter estimation, parity equations or state observers. The faults are also evaluated by means of tri-valued and fuzzy information system approaches (see more details in [18, 19, 20, 21, 22]). Fault diagnosis is typically achieved by combining a residual generator and a residual evaluation strategy to provide logical statements on whether faults have occurred. Marzat et al. [23] presented a survey of model-based fault diagnosis, which summarizes on those methods that are applicable to aerospace systems. The authors of [24] show how SMCs can be exploited for fault detection (specifically fault signal estimation) and subsequently fault tolerant control, including an aerospace application. Combinations of the SMCs and sliding-mode observers/differentiators (SMDs) are considered in [25, 26, 27, 28, 29], these algorithms are designed to detect on-line and reconstruct the faults, ensuring a tolerance to a wide class of additive failures.

Recently, FDI results for the 3-DoF helicopter prototype were reported in [30] where the usage of residual-based equations is suggested. The scheme is based on a linear observer and the reconstruction of the acceleration through a sliding mode differentiator. The well-known Super-Twisting Algorithm (STA) [31] is used to steer the system states to erroneously estimated trajectories (due to unknown inputs (faults) affecting observer's error).

On the other hand, controllers based on the Super-Twisting Algorithm (STA) [31] and the Continuous Twisting Algorithm (CTA) [32] are developed in [33] to reach sliding surfaces of relative degree one and two. A FDI procedure based on sliding-mode differentiators is given and tested by simulations only. Moreover, they can not ensure the best possible accuracy taking into account the dynamics

of motors [7].

In this paper, FTCs based on the recently developed Continuous Twisting Algorithm (CTA) [32, 34] are designed, ensuring acceptable performance of the helicopter in presence of faults in the motors. Residual-based equations are constructed in order to detect and isolate the faults by using SMDs, [35]. A comparison with respect a classic observer-based FDI procedure is given to highlight the advantages of proposal. This paper is focused on fault detection and isolation in the motors of a 3-DoF Helicopter prototype using residual equations, that are constructed from the systems model, the measurements of inputs and the outputs (and its time-derivatives). Sensor faults can be detected in systems with redundancy of measurements as proposed by [24]. However, there are only one sensor installed in the helicopter prototype for each degree of freedom. Then, it is not possible to construct residuals in order to detect sensors faults with the available hardware, [25].

1.1. Main contributions

In this paper, the CTA is used to ensure robust stabilization of a 3-DoF helicopter prototype in presence of actuator faults. With this approach,

1. A residual-based FDI procedure is given using the available information, i.e. the output, and some of its derivatives, which are provided in finite-time by a robust sliding-mode differentiator.

2. Tuning rules for thresholds allowing the adjustment of model's parameters.

The effectiveness of our proposal is tested both with extensive simulations and on the experimental setup.

1.2. Structure of the Paper

In Section 2 the model of the 3-DoF helicopter prototype is presented. FTCs, based on the Continuous Twisting algorithm, are developed in Section 3. The high-order SMD and the residual-based equations are given in Section 4. Simulation results are shown in Section 5. A comparison with a classic observer-based

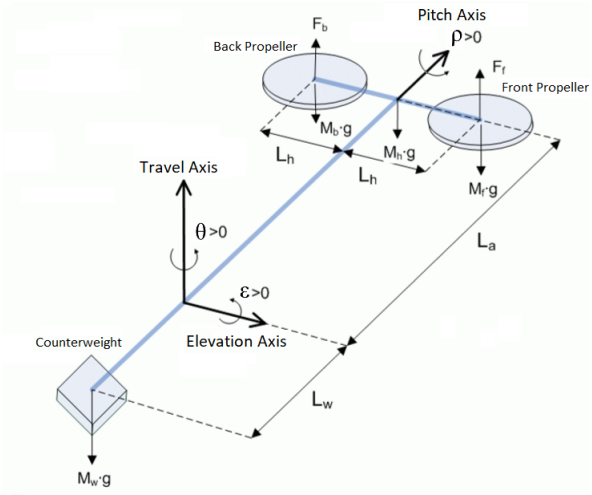

Figure 1: Free-body diagram of the 3-DoF helicopter prototype.

FDI procedure is proposed in Section 6. Experimental results are reported in Section 7. Finally, Section 8 summarizes the conclusions of the paper.

2. System Description and Problem Statement

2.1. Mathematical model of the 3-DoF helicopter prototype

The 3-DoF helicopter prototype consists of an arm with two DC motors, mounted at one of the frame end. A counterweight mass is in the opposite side of the frame. The DC motors provide the lift forces F_f and F_b (which are assumed proportional to the voltage V_f and V_b, respectively). The system can rotate freely about three axes: elevation angle ε, pitch angle ρ and travel angle θ, as shown in Fig. 1. The model of the 3-DoF helicopter is given by the second-order differential equations [1],

$$\ddot{\varepsilon} = \frac{1}{J_\varepsilon}\Big(K_f L_a \cos(\rho)\big(V_f + V_b\big) + g\cos(\varepsilon)\big(M_w L_w - M_h L_a\big)\Big)\,, \tag{1a}$$

$$\ddot{\rho} = \frac{K_f L_h}{J_\rho}\big(V_f - V_b\big)\,, \tag{1b}$$

$$\ddot{\theta} = -\frac{K_f L_a}{J_\theta}\sin(\rho)\,\big(V_f + V_b\big)\,, \tag{1c}$$

where J_ε, J_ρ, J_θ are the moments of inertia about the elevation, pitch and travel axes, respectively. L_a is the distance from the travel axis to the helicopter body, L_h is the distance from the pitch axis to any of the motors. M_h is the total mass of the helicopter body, M_w is the mass of the counterweight, L_w is the distance from the travel axis to the counterweight, and g is the gravity acceleration. K_f represents the ratio between the lift forces F_f, F_b, and the voltages V_f, V_b. In addition, friction and aerodynamics drag effects are neglected. The position of the helicopter body is given by the elevation ε, pitch ρ and travel θ angles. The *workspace*[1] is summarized in Table 1. Also, the operating voltage of the DC motors in the propellers is included in Table 1. Values of the model parameters are in Table 2. The states (ε,ρ,θ) are the only measurements of the system available for control.

2.2. Definition of Faults

Faults in motors of the 3-DoF helicopter can be caused by several factors, such as overheating, short circuit, mechanical wear and discrepancies in power supplies and control stages, to mention a few. In this paper a fault in the front

[1]The workspace of the 3-DoF helicopter prototype is the total volume swept out by the helicopter body as the propellers execute all possible motions.

Table 1: Variables of the 3-DoF Helicopter

Variable	Interval	Unit	Description
ε	$[-25,\ 25]$	$^\circ$	Variation of the elevation angle
ρ	$[-90,\ 90]$	$^\circ$	Variation of the pitch angle
θ	$(-\infty, \infty)$	$^\circ$	Variation of the travel angle
V_f	$[-12, 12]$	V	Operating voltage of the front motor
V_b	$[-12, 12]$	V	Operating voltage of the back motor

motor is modeled as a voltage drop,

$$V_f^* = \begin{cases} V_f & \text{if} \quad t < t_f \,, \\ \gamma_f V_f & \text{if} \quad t \geq t_f \,, \end{cases} \tag{2}$$

where t_f is a time when the voltage drops in the front motor, and $0 < \gamma_f < 1$ is a constant value which expresses the percentage of fault. In a similar way, a fault in the back motor is defined by

$$V_b^* = \begin{cases} V_b & \text{if} \quad t < t_b \,, \\ \gamma_b V_b & \text{if} \quad t \geq t_b \,, \end{cases} \tag{3}$$

Remark 1. *Definitions (2) and (3) are for abrupt faults, i.e. step-changes in the voltage supplied to the motors, at times t_f and t_b, respectively. However, intermittent, oscillatory and incipient faults can be considered as suggested in [29].*

2.3. Problem Statement

The goal of the paper is to develop a fault-tolerant controller for the 3-DoF helicopter prototype modeled by the Eqs. (1a)-(1b)-(1c), in order to drive the

Table 2: Model parameters

Parameter	Value	Unit	Description
J_ε	0.91	kgm^2	Inertial moment around the elevation axis
J_ρ	0.0364	kgm^2	Inertial moment around the pitch axis
J_θ	0.91	kgm^2	Inertial moment around the travel axis
K_p	0.686	N	Flight constant
K_f	0.1188	N/V	Force-Voltage propellers constant
M_h	1.15	kg	Helicopter total mass
M_w	1.87	kg	Counterweight mass
L_a	0.66	m	Helicopter-travel axis length
L_h	0.177	m	Propeller-pitch axis length
L_w	0.47	m	Counterweight-travel axis length
g	9.81	m/s^2	Gravity acceleration

trajectories of the closed-loop system to the origin even in the presence of faults (2)-(3). With this aim, a fault-tolerant control based on the recently developed Continuous Twisting Algorithm (CTA) [32, 34] is implemented, able to mitigate consequences of faults in the actuators of a 3-DoF helicopter prototype. Let a sliding variable $s \in \mathbb{R}$ of relative degree $r > 0$, the CTA controller is defined as

$$\begin{aligned} u &= -k_1 \lfloor s \rceil^{\frac{1}{r+1}} - k_2 \lfloor \dot{s} \rceil^{\frac{1}{r}} - \ldots - k_r \lfloor s^{(r-1)} \rceil^{\frac{1}{2}} + v \,, \\ \dot{v} &= -k_{r+1} \lfloor s \rceil^{0} - k_{r+2} \lfloor \dot{s} \rceil^{0} - \ldots - k_{2r} \lfloor s^{(r-1)} \rceil^{0} \,, \end{aligned} \tag{4}$$

where $k_i > 0$, $i = 1, ..., 2r$, are the gains of the controller. The nonlinear terms are defined as $\lfloor \cdot \rceil^p = |\cdot|^p \text{sign}(\cdot)$ with power $0 < p < 1$. The CTA has the following advantages:

- It is able to drive a disturbed SISO system of relative degree $r > 0$ from the measurements of the outputs $s \in \mathbb{R}$ (sliding variable) and their $r - 1$ time derivatives.
- The CTA algorithm provides finite-time stabilization of the outputs s and their r time derivatives to the origin, all at the same time.
- It generates a continuous control signal.
- The CTA controller compensates (theoretically exactly) matched Lipschitz perturbations.
- The output s has $(r+1)$-sliding accuracy in presence of parasitic dynamics, i.e. $|s| \leq \gamma \, \mu^{r+1}$ for some $\gamma > 0$, after a transient process. The parameter $\mu > 0$ represents the time constant of some parasitic dynamics, e.g. actuators, sensors, delays (see more details in [7]).

The use of CTA in FTCs provides robust stabilization of the system trajectories to the sliding set $s = \dot{s} = ... = s^{(r)} = 0$, by means of continuous control signals. CTA controllers for relative degree two (for the elevation subsystem) and relative degree three (for the pitch-travel subsystem) are chosen in order to improve accuracy of the sliding variable in presence of fast-parasitic dynamics, e.g. the actuators of the system. A fault detection and isolation scheme is proposed

through residual-based equations that require the availability of the system acceleration information. In order to have a sensorless procedure, a third-order sliding mode differentiator [35] is used not only to obtain the accelerations, but also to complete the state vector (the helicopter velocities). The effectiveness of our proposal is tested both with extensive simulations and on the experimental setup.

3. State Feedback Sliding Mode Control

3.1. Linearized model of the 3-DoF helicopter dynamics

Given the state vector $x = [\varepsilon, \rho, \theta, \dot{\varepsilon}, \dot{\rho}, \dot{\theta}]^\top$, an operation point of the system is defined as any feasible trajectory such that $X = [\bar{\varepsilon}, 0, \bar{\theta}, 0, 0, 0]^\top$, where $(\bar{\varepsilon}, \bar{\theta})$ are desired angles into the *workspace* (see Table 1). Considering the control inputs

$$u_s = V_f + V_b \,, \tag{5a}$$

$$u_d = V_f - V_b \,, \tag{5b}$$

the control vector $u = [u_s, u_d]^\top$ at any operating point X is such that $U = [-\frac{\tau_g \cos(\bar{\varepsilon})}{K_f L_a}, 0]^\top$ with $\tau_g = g(M_w L_w - M_h L_a)$ the gravitational torque around the elevation axis. Then, the linearized model of the 3-DoF helicopter dynamics (1a)-(1b)-(1c) around the operating point (X, U) has the form

$$\dot{x} = \begin{bmatrix} 0 & 0 & 0 & 1 & 0 & 0 \\ 0 & 0 & 0 & 0 & 1 & 0 \\ 0 & 0 & 0 & 0 & 0 & 1 \\ -\frac{\tau_g \sin(\bar{\varepsilon})}{J_\varepsilon} & 0 & 0 & 0 & 0 & 0 \\ 0 & 0 & 0 & 0 & 0 & 0 \\ 0 & \frac{\tau_g \cos(\bar{\varepsilon})}{J_\theta} & 0 & 0 & 0 & 0 \end{bmatrix} x + \begin{bmatrix} 0 & 0 \\ 0 & 0 \\ 0 & 0 \\ \frac{K_f L_a}{J_\varepsilon} & 0 \\ 0 & \frac{K_f L_h}{J_\rho} \\ 0 & 0 \end{bmatrix} u \,, \tag{6}$$

with the measured output

$$y = \begin{bmatrix} 1 & 0 & 0 & 0 & 0 & 0 \\ 0 & 1 & 0 & 0 & 0 & 0 \\ 0 & 0 & 1 & 0 & 0 & 0 \end{bmatrix} x \,. \tag{7}$$

CTA-based controller for the Elevation dynamics

The linearized model (6) can be rewritten as two subsystems. Let the state vector $x_1 = [\varepsilon, \dot{\varepsilon}]^\top$, the subsystem related to the elevation dynamics has the form

$$\begin{aligned} \dot{x}_1 &= \underbrace{\begin{bmatrix} 0 & 1 \\ -\frac{\tau_g \sin(\bar{\varepsilon})}{J_\varepsilon} & 0 \end{bmatrix}}_{A_1} x_1 + \underbrace{\begin{bmatrix} 0 \\ \frac{K_f L_a}{J_\varepsilon} \end{bmatrix}}_{B_1} u_s \,, \\ y_1 &= \underbrace{\begin{bmatrix} 1 & 0 \end{bmatrix}}_{C_1} x_1 \,. \end{aligned} \tag{8}$$

The dynamical system (8) is of relative degree $r_1 = 2$ from the output $y_1 = \varepsilon$ to the control input u_s, i.e.

$$\ddot{\varepsilon} = \frac{K_f L_a}{J_\varepsilon} u_s - \frac{\tau_g \sin(\bar{\varepsilon})}{J_\varepsilon} \varepsilon \,. \tag{9}$$

Let the input

$$u_s = \frac{J_\varepsilon}{K_f L_a} \left(u_1 + \frac{\tau_g \sin(\bar{\varepsilon})}{J_\varepsilon} \varepsilon \right) + u_{s_{eq}} \,, \tag{10}$$

where the term u_1 is based on CTA (4), then

$$u_1 = -k_{11} \lfloor \varepsilon \rceil^{\frac{1}{3}} - k_{12} \lfloor \dot{\varepsilon} \rceil^{\frac{1}{2}} + v_1 \,, \tag{11a}$$

$$\dot{v}_1 = -k_{13} \lfloor \varepsilon \rceil^0 - k_{14} \lfloor \dot{\varepsilon} \rceil^0 \,, \tag{11b}$$

the parameters of the controller $k_{11}, k_{12}, k_{13}, k_{14} > 0$ are chosen to enforce third-order sliding-modes, i.e. there exist a finite time t_{r_1} such that $\varepsilon(t) = \dot{\varepsilon}(t) = \ddot{\varepsilon}(t) = 0$ for all $t \geq t_{r_1}$ (see more details in [32]). Note that controller (10) contains the voltage at the equilibrium point $u_{s_{eq}} = -\frac{\tau_g \cos(\bar{\varepsilon})}{K_f L_a}$, in order to improve the transient process.

CTA-based Controller for the Pitch-Travel Dynamics

The other subsystem is related to the pitch-travel dynamics. Consider the state vector $x_2 = [\rho, \theta, \dot{\rho}, \dot{\theta}]^\top$, then

$$\begin{aligned} \dot{x}_2 &= \underbrace{\begin{bmatrix} 0 & 0 & 1 & 0 \\ 0 & 0 & 0 & 1 \\ 0 & 0 & 0 & 0 \\ \frac{\tau_g \cos(\bar{\varepsilon})}{J_\theta} & 0 & 0 & 0 \end{bmatrix}}_{A_2} x_2 + \underbrace{\begin{bmatrix} 0 \\ 0 \\ \frac{K_f L_h}{J_\rho} \\ 0 \end{bmatrix}}_{B_2} u_d \,, \\ y_2 &= \underbrace{\begin{bmatrix} 1 & 0 & 0 & 0 \\ 0 & 1 & 0 & 0 \end{bmatrix}}_{C_2} x_2 \,. \end{aligned} \tag{12}$$

The dynamical system (12) is of relative degree $r_2 = 3$ from the output $s = \dot{\theta} + c\,\theta$ to the control input u_d, i.e.

$$\dot{s} = c\,\dot{\theta} + \frac{\tau_g \cos(\bar{\varepsilon})}{J_\theta}\rho \,, \tag{13a}$$

$$\ddot{s} = \frac{c\tau_g \cos(\bar{\varepsilon})}{J_\theta}\rho + \frac{\tau_g \cos(\bar{\varepsilon})}{J_\theta}\dot{\rho} \,, \tag{13b}$$

$$s^{(3)} = \frac{c\tau_g \cos(\bar{\varepsilon})}{J_\theta}\dot{\rho} + \left(\frac{\tau_g \cos(\bar{\varepsilon})}{J_\theta}\right)\left(\frac{K_f L_h}{J_\rho}\right) u_d \,. \tag{13c}$$

Let the input

$$u_d = \frac{J_\theta J_\rho}{\tau_g \cos(\bar{\varepsilon}) K_f L_h}\left(u_2 - \frac{c\tau_g \cos(\bar{\varepsilon})}{J_\theta}\dot{\rho}\right) \,, \tag{14}$$

where the term u_2 is based on CTA (4), then

$$u_2 = -k_{21}\lfloor s \rceil^{\frac{1}{4}} - k_{22}\lfloor \dot{s} \rceil^{\frac{1}{3}} - k_{23}\lfloor \ddot{s} \rceil^{\frac{1}{2}} + v_2 \,, \tag{15a}$$

$$\dot{v}_2 = -k_{24}\lfloor s \rceil^0 - k_{25}\lfloor \dot{s} \rceil^0 - k_{26}\lfloor \ddot{s} \rceil^0 \,, \tag{15b}$$

the parameters of the controller $k_{21}, k_{22}, k_{23}, k_{24}, k_{26}, k_{26} > 0$ are chosen to enforce fourth-order sliding-modes, i.e. there exist a finite time t_{r_2} such that $s(t) = \dot{s}(t) = \ddot{s}(t) = s^{(3)}(t) = 0$ for all $t \geq t_{r_2}$ (see more details in [34]). Note that into sliding modes the reduced order dynamics has the form

$$\theta(t) = \theta(0)\, e^{-ct} \,, \tag{16}$$

with initial condition $\theta(0) \in \mathbb{R}$. Then, any $c > 0$ ensure exponentially stability of the zero dynamics, nevertheless, an appropriate selection of $c > 0$ should avoid excessive tilt of the pitch angle (which could cause lost of altitude).

Remark 2. *A saturated version of CTA controller [36, 37, 38] can be implemented in order to avoid instability caused by the change of rotation of the helicopter propellers and saturation of control signals due to the .*

4. Residual-Based FDI Scheme

Proposition 1. *Consider the residual-based equations constructed by the measurements of the accelerations and the control inputs,*

$$R_\varepsilon = \frac{J_\varepsilon \ddot{\varepsilon} - \tau_g \cos(\varepsilon)}{K_f L_a \cos(\rho)} - u_s \,, \tag{17a}$$

$$R_\rho = \frac{J_\rho}{K_f L_h} \ddot{\rho} - u_d \,. \tag{17b}$$

Table 3: Residual detectors (17a)-(17b) and FDI equations (18a)-(18b) in presence of the faults (2)-(3).

	Fault in Front (V_f^*)	Fault in Back (V_b^*)	Simultanuous Faults (V_f^*, V_b^*)
R_ε	$-\left(1-\frac{1}{\gamma_f}\right)V_f$	$-\left(1-\frac{1}{\gamma_b}\right)V_b$	$-\left(1-\frac{1}{\gamma_f}\right)V_f-\left(1-\frac{1}{\gamma_b}\right)V_b$
R_ρ	$-\left(1-\frac{1}{\gamma_f}\right)V_f$	$\left(1-\frac{1}{\gamma_b}\right)V_b$	$-\left(1-\frac{1}{\gamma_f}\right)V_f+\left(1-\frac{1}{\gamma_b}\right)V_b$
R_f	$-2\left(1-\frac{1}{\gamma_f}\right)V_f$	0	$-2\left(1-\frac{1}{\gamma_f}\right)V_f$
R_b	0	$-2\left(1-\frac{1}{\gamma_b}\right)V_b$	$-2\left(1-\frac{1}{\gamma_b}\right)V_b$

The isolation procedure consists of operating with the residual-based equations (17a) and (17b), in order to know in which motor the fault occurred and in what time, even if the faults occur at the same time. The fault detector of the front motor is constructed with the sum between the residual-based equations (17a) and (17b). The fault detector of the back motor is constructed with the difference between the residual-based equations (17a) and (17b). Then, the FDI equations are

$$R_f = R_\varepsilon + R_\rho \,, \tag{18a}$$

$$R_b = R_\varepsilon - R_\rho \,, \tag{18b}$$

for the front motor (18a) and for the back motor (18b).

More details about the Proposition 1 are in the Appendix section. Table 3 summarizes the logical states established in presence of faults: second column of isolated faults in the front motor, third column of isolated faults in the back motor, and fourth column of simultaneous faults in both motors.

4.1. High-Order Sliding Mode Differentiator

To implement the controllers and to detect and isolate the faults, the angular position, velocity and acceleration around the elevation, pitch and travel axes are required. A third-order sliding mode differentiator is designed for robust differentiation of angular positions in presence of measurement noises. The structure of differentiator is as follows [35],

$$\begin{aligned}
\dot{z}_0 &= -\lambda_3 L^{\frac{1}{4}} \lfloor z_0 - y \rceil^{\frac{3}{4}} + z_1 \,, \\
\dot{z}_1 &= -\lambda_2 L^{\frac{1}{3}} \lfloor z_1 - \dot{z}_0 \rceil^{\frac{2}{3}} + z_2 \,, \\
\dot{z}_2 &= -\lambda_1 L^{\frac{1}{2}} \lfloor z_2 - \dot{z}_1 \rceil^{\frac{1}{2}} + z_3 \,, \\
\dot{z}_3 &= -\lambda_0 L \lfloor z_3 - \dot{z}_2 \rceil^{0} \,,
\end{aligned} \tag{19}$$

with the parameters $\lambda_0 = 1.1$, $\lambda_1 = 1.5$, $\lambda_2 = 3$, $\lambda_3 = 5$, and the scaling matrix $L = \text{diag}\{L_\varepsilon, L_\rho, L_\theta\} > 0$. Thus, the velocity vector $z_1 = [\dot{\varepsilon} \;\; \dot{\rho} \;\; \dot{\theta}]^\top$ and the acceleration vector $z_2 = [\ddot{\varepsilon} \;\; \ddot{\rho} \;\; \ddot{\theta}]^\top$ are computed in finite-time from the measurements of the angles $y = [\varepsilon \;\; \rho \;\; \theta]^\top$.

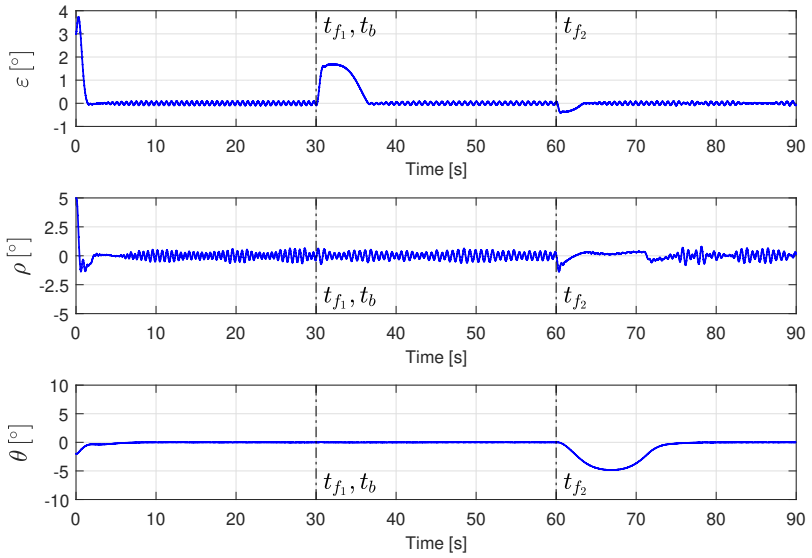

Figure 2: Angular positions of the 3-DoF helicopter prototype with CTA control laws (10) and (14): simulation results.

5. Simulation Results

The simulation framework consists of a Matlab/Simulink environment in which the differential equations (1a)-(1b)-(1c) are solved by using the Euler's integration method (ODE1) with fixed step $\tau = 1 \times 10^{-4}$ seconds. The initial conditions are $x(0) = [3, 5, -2, 0, 0, 0]^\top$ degrees. The faults are induced by software after the settling time from the initial conditions. An intermittent fault is forced in the front motor at time $t_{f_1} = 30$ seconds which stops at time $t_{f_2} = 60$ seconds. On the back motor a persistent fault appears at time $t_b = 30$ seconds and it remains throughout the simulation. In both cases, 30% of drop voltage due to failures are considered, i.e. $\gamma_f = \gamma_b = 0.7$. In addition, bounded white noise of magnitude 3×10^{-4} is added to all the position measurements in order to emulate conditions similar to a real measurement environment. Parasitic dynamics are all dynamical components that are not considered in the model of the system used for control designing. In this paper, the actuators dynamics are not considered in the design-step of CTA controllers. They are considered

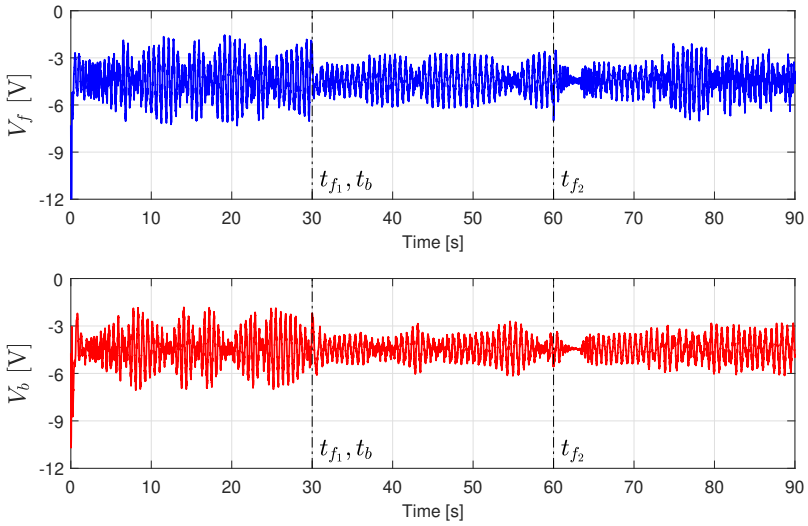

Figure 3: Voltage in motors with CTA control laws (10) and (14): simulation results.

the main reason of chattering [7]. The actuators (DC motors with attached propellers) are modeled as first-order differential equations

$$\mu \dot{F}_f + F_f = K_f V_f \quad \text{and} \quad \mu \dot{F}_b + F_b = K_f V_b \,, \tag{20}$$

with time constant $\mu = 0.2$, about twenty times the inertia of the rotor Pittman 9234S004 without load.

The gains of the controller defined by Eqn. (10) were taken from the Eqn. (8) in paper [32]. The gains of the controller in Eqn. (14) were taken from the Table 1 in paper [34]. Both sets of gains were adjusted in order to have a desired closed-loop performance. Thus, the gains of the controller (10) are chosen $k_{11} = 1.2$, $k_{12} = 2.2$, $k_{13} = 0.1$ and $k_{14} = 0$. On the other hand, the gains of the controller (14) are selected $k_{21} = 3$, $k_{22} = 5$, $k_{23} = 8$, $k_{24} = 0.3$, $k_{25} = 0$ and $k_{26} = 0$. Also, the parameter of the sliding variable is fixed $c = 0.5$. Fig. 2 shows the angular positions of the 3-DoF helicopter prototype, it can be seen that CTA controllers are able to drive the trajectories to a vicinity of the origin, even in presence of faults. The voltage of the motors that mitigates consequences of faults in the actuators of a 3-DoF helicopter prototype are in Fig. 3. The residual based equations of the front (18a) and the back (18b)

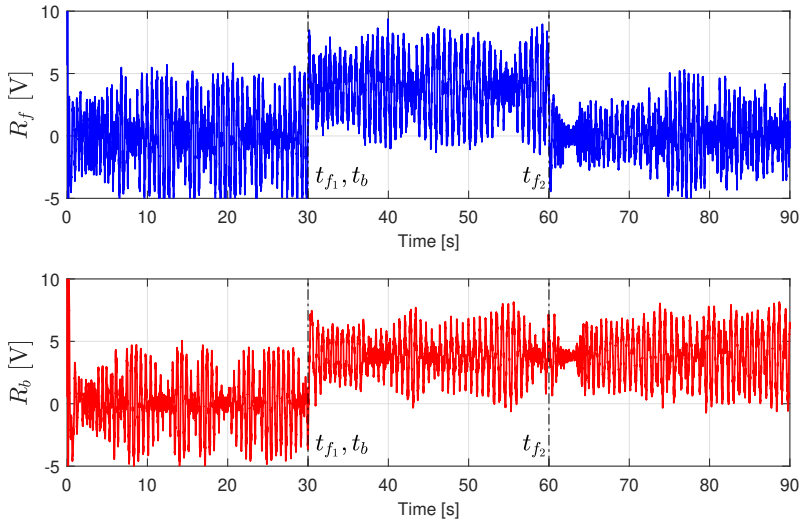

Figure 4: FDI signals (18a) and (18b) measured from the experimental setup with CTA control laws (10) and (14): simulation results.

motors are shown in Fig. 4. An intermittent fault in the front motor of duration $T = t_{f_2} - t_{f_1} = 30$ seconds is detected by the residual (18a), a persistent fault in the back motor is detected by the residual (18b) from time $t_b = 30$ seconds, until the end of the simulation.

5.1. Thresholds Adjustment

Lack of knowledge of some parameters in the model given by the equations (1a)-(1b)-(1c) cause offset levels in the residual-based detectors (18a)-(18b) in absence of faults. However, some of those parameters are easy to measure as the masses, lengths and inertial moments. On the other hand, the ratio between the lifting forces and the voltage in motors (K_f parameter) is hardly-dependent on deteriorating conditions of the DC motors and propellers. Considering for example, $K_f = 0.2$ N/V as the true parameter of the system, but the controllers (10), (14), and the residual-based generators (18a)-(18b), are designed taking into account: (i) $K_f = 0.4$ N/V; (ii) $K_f = 0.3$ N/V; (iii) $K_f = 0.2$ N/V (the true parameter). Figure 5 shows the residual-based equations (18a)-(18b) obtained by simulations: (left) $K_f = 0.4$ N/V; (center) $K_f = 0.3$ N/V; (right) $K_f = 0.2$

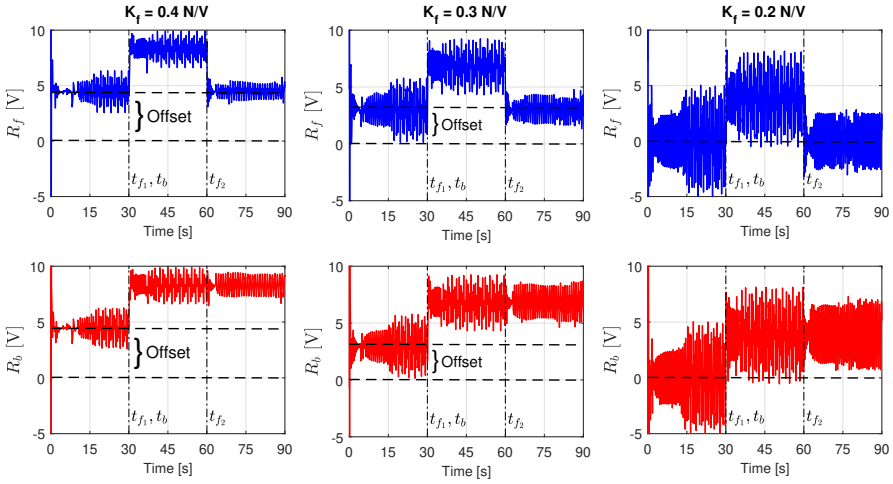

Figure 5: Tuning of thresholds for residual-based detection and isolation of faults: simulation results.

N/V. The residual detectors (18a)-(18b) are shifted over zero due to lack of knowledge on K_f parameter (see Fig. 5 at left and center), which imply false-positives in the FDI procedure. However, it is possible to adjust these offset levels tuning the K_f parameter (there are no offset in Fig. 5 at right when K_f parameter is well known). Note that sliding-mode controllers drive the system trajectories to zero despite the lack of knowledge of K_f parameter, only the transient response is affected by the variation of it.

5.2. Analysis of simulation results

- The controllers based on CTA drive the trajectories to zero even in presence of faults, modeled as (2)-(3), in the motors of the 3-DoF helicopter prototype.

- The residual-based equations in Fig. (4) allow to detect and to isolate faults in the motors of the 3-DoF helicopter prototype, even if they occur at the same time.

- The offset levels in the residual equations (18a)-(18b) can be mitigated by tuning the K_f parameter in the model (1a)-(1b)-(1c). The CTA con-

trollers drive to zero the states of the helicopter, even with the parametric uncertainty of K_f.

- It can be seen fast-oscillations (chattering) in a vicinity of the origin caused by the presence of unmodeled dynamics, in this case, due to the the actuator dynamics modeled by (20).

- The noise in the measurements strongly affects the residual detectors (18a)-(18b) as can be seen in Fig. 4. However, filtering of such residuals is suggested in order to mitigate the consequences of the noise.

6. Comparison with respect to a classic observer-based FDI scheme

A fair comparison of the proposed method with other robust FDI procedures should be considered to develop a dynamical system, in order to detect the faults and also to complete the states required by the feedback controllers. The usage of sliding mode observers for FDI has been strongly studied due to its capability to reconstruct (online) unmeasurable signals by filtering of the so-called equivalent output error injection [39, 25, 24]. By way of comparison, a classical FDI scheme based on sliding-mode observers is developed combined with the previously designed CTA controllers. The observer-based FDI scheme is able to drive the trajectories of the system to zero, even in presence of faults in the actuators of the 3-DoF helicopter prototype. The operations proposed in Section 4 are used to isolate the faults in the actuation system.

6.1. Observer-based FD scheme for the elevation dynamics

Considering the subsystem (8) related to the elevation dynamics, for a given output matrix C_1, the pair (B_1, C_1) must satisfy the condition $\text{rank}(C_1 B_1) = 1$ to build an unknown input observer [25]. Then, the following output matrix is suggested

$$C_1 = \begin{bmatrix} 1 & 1 \end{bmatrix}, \tag{21}$$

note that output matrix (21) implies the measurement of $\dot{\varepsilon}$. Using an algorithm similar to the one proposed in [39], it can be shown that the transformation matrix

$$T_1 = \begin{bmatrix} 2 & 0 \\ 1 & 1 \end{bmatrix},$$

allows to rewrite the model (8) in *canonical form*, i.e.

$$\bar{A} = T_1 A_1 T_1^{-1} = \left[\begin{array}{c|c} -1 & 2 \\ \hline -\frac{1}{2}\left(\frac{\tau_g \sin(\bar{\varepsilon})}{J_\varepsilon} + 1\right) & 1 \end{array}\right],$$
$$\bar{B} = T_1 B_1 = \left[\begin{array}{c} 0 \\ \hline \frac{K_f L_a}{J_\varepsilon} \end{array}\right]; \quad \bar{C} = C_1 T_1^{-1} = \left[\begin{array}{c|c} 0 & 1 \end{array}\right].$$

In this case, $\bar{A}_{11} = -1$, $\bar{A}_{12} = 2$, $\bar{A}_{21} = -\frac{1}{2}\left(\frac{\tau_g \sin(\bar{\varepsilon})}{J_\varepsilon} + 1\right)$, $\bar{A}_{22} = 1$, $\bar{B}_2 = \frac{K_f L_a}{J_\varepsilon}$ and $\bar{C}_2 = 1$. The objective is to design an observer to estimate the state $\hat{x}_1$ such that a sliding mode is attained in which the output error $e_{y_1} = C_1\hat{x}_1 - y_1$ is driven to zero in finite time, even in the presence of the faults (2)-(3). The particular observer that will be considered has the form

$$\dot{\hat{x}}_1 = A_1\hat{x}_1 + B_1(u_s + u_{s_{eq}}) - G_{l1}e_{y_1} + G_{n1}\nu_1, \tag{22}$$

with error injection matrices

$$G_{l1} = T_1^{-1}\begin{bmatrix} \bar{A}_{12} \\ \bar{A}_{22} - \bar{A}_{22}^s \end{bmatrix}; \quad G_{n1} = T_1^{-1}\begin{bmatrix} 0 \\ 1 \end{bmatrix}.$$

where $\bar{A}_{22}^s$ is selected such that $P_1\bar{A}_{22}^s + \bar{A}_{22}^\top P_1 = -1$ with $P_1 > 0$. The nonlinear error injection is defined as

$$\nu_1 = -\rho_1 \operatorname{sign}(P_1 e_{y_1}), \tag{23}$$

with $\rho_1 > 0$. Note that $e_{y_1} = \dot{e}_{y_1} = 0$, then the error dynamics has the form

$$\begin{aligned} \dot{e}_1 = &\quad \bar{A}_{11}e_1, \\ 0 = &\quad \bar{A}_{21}e_1 + \bar{B}_2 f_s + \nu_{1_{eq}}, \end{aligned}$$

where f_s is an unknown input and $\nu_{1_{eq}}$ is the so-called equivalent output injection signal and represents the average behaviour of the discontinuous component

necessary to maintain the motion on the sliding surface [2]. Since $\bar{A}_{11}$ is stable and $e_1 \to 0$, it follows that $\nu_{1_{eq}} \to -\bar{B}_2 f_s$ asymptotically. Also $\text{rank}(\bar{B}_2) = 1$, it implies

$$f_s = -(\bar{B}_2^\top \bar{B}_2)^{-1} \bar{B}_2^\top \nu_{1_{eq}} = -\frac{J_\varepsilon}{K_f L_a} \nu_{1_{eq}} \,. \tag{24}$$

The right-hand side of the equation above can be computed on-line since it only depends on the output estimation error e_{y_1}. It is possible to obtain $\nu_{1_{eq}}$ by filtering the discontinuous term ν_1 in (23) and then to detect the fault f_s.

6.2. Observer-based FD scheme for the pitch-travel dynamics

Considering the subsystem (12) related to the pitch-travel dynamics, for a given output matrix C_2, the pair (B_2, C_2) must satisfy the condition $\text{rank}(C_2 B_2) = 1$, to build an unknown input observer [25]. Then, the following output matrix is suggested

$$C_2 = \begin{bmatrix} 1 & 0 & 1 & 0 \\ 0 & 1 & 0 & 0 \end{bmatrix} . \tag{25}$$

Note that the output matrix (21) implies the measurement of $\dot{\rho}$. Using an algorithm similar to that proposed in [39], it can be shown that the transformation matrix

$$T_2 = \begin{bmatrix} 2 & 2 & 0 & 0 \\ -2 & 11 & 0 & -1 \\ 1 & 0 & 1 & 0 \\ 0 & 1 & 0 & 0 \end{bmatrix} ,$$

allows to rewrite the model (12) in *canonical form*, i.e.

$$\bar{A} = T_2 A_2 T_2^{-1} = \left[\begin{array}{cc|cc} -3 & -2 & 2 & 28 \\ -(\frac{\tau_g \cos(\bar{\varepsilon})}{2J_\theta} + 10) & -11 & -2 & \frac{\tau_g \cos(\bar{\varepsilon})}{J_\theta} + 141 \\ \hline -0.5 & 0 & 1 & 1 \\ -1 & -1 & 0 & 13 \end{array}\right] ,$$

$$\bar{B} = T_2 B_2 = \left[\begin{array}{c} 0 \\ 0 \\ \hline \frac{K_f L_h}{J_\rho} \\ 0 \end{array}\right] \; ; \; \bar{C} = C_2 T_2^{-1} = \left[\begin{array}{cc|cc} 0 & 0 & 1 & 0 \\ 0 & 0 & 0 & 1 \end{array}\right] .$$

In this case, $\bar{A}_{11} = \begin{bmatrix} -3 & -2 \\ -(\frac{\tau_g \cos(\bar{\varepsilon})}{2J_\theta} + 10) & -11 \end{bmatrix}$, $\bar{A}_{12} = \begin{bmatrix} 2 & 28 \\ -2 & \frac{\tau_g \cos(\bar{\varepsilon})}{J_\theta} + 141 \end{bmatrix}$, $\bar{A}_{21} = \begin{bmatrix} -0.5 & 0 \\ -1 & -1 \end{bmatrix}$, $\bar{A}_{22} = \begin{bmatrix} 1 & 1 \\ 0 & 13 \end{bmatrix}$, $\bar{B}_2 = \begin{bmatrix} \frac{K_f L_h}{J_\rho} \\ 0 \end{bmatrix}$ and $\bar{C}_2 = I_2 = \begin{bmatrix} 1 & 0 \\ 0 & 1 \end{bmatrix}$. The objective is to design an observer to estimate the state $\hat{x}_2$ such that a sliding mode is attained in which the output error $e_{y_2} = C_2\hat{x}_2 - y_2$ is driven to zero in finite time, even in the presence of the faults (2)-(3). The observer has the form

$$\dot{\hat{x}}_2 = A_2\hat{x}_2 + B_2 u_d - G_{l2} e_{y_2} + G_{n2}\nu_2 \,, \tag{26}$$

with error injection matrices

$$G_{l2} = T_2^{-1} \begin{bmatrix} \bar{A}_{12} \\ \bar{A}_{22} - \bar{A}_{22}^s \end{bmatrix} \;;\; G_{n2} = T_2^{-1} \begin{bmatrix} 0 \\ I_2 \end{bmatrix} .$$

where $\bar{A}_{22}^s$ is chosen such that $P_2\bar{A}_{22}^s + \bar{A}_{22}^{s\top} P_2 = -I_2$ with $P_2 = P_2^\top > 0$. The non-linear error injection is defined as

$$\nu_2 = \begin{bmatrix} -\rho_{21}\,\mathrm{sign}(P_{2_{11}} e_{y_{21}} + P_{2_{12}} e_{y_{22}}) & -\rho_{22}\,\mathrm{sign}(P_{2_{21}} e_{y_{21}} + P_{2_{22}} e_{y_{22}}) \end{bmatrix}^\top , \tag{27}$$

with $\rho_{21}, \rho_{22} > 0$. Note that $e_{y_2} = \dot{e}_{y_2} = \bar{0}$, then the error dynamics has the form

$$\begin{aligned} \dot{e}_1 = &\quad \bar{A}_{11} e_1 \,, \\ 0 = &\quad \bar{A}_{21} e_1 + \bar{B}_2 f_d + \nu_{2_{eq}} \,, \end{aligned}$$

where f_s is an unknown input and $\nu_{2_{eq}}$ is the so-called equivalent output injection signal. Since $\bar{A}_{11}$ is stable, $e_1 \to 0$, it follows that $\nu_{2_{eq}} \to -\bar{B}_2 f_d$ asymptotically. Also $\mathrm{rank}(\bar{B}_2) = 1$, it implies

$$f_d = -(\bar{B}_2^\top \bar{B}_2)^{-1} \bar{B}_2^\top \nu_{2_{eq}} = -\begin{bmatrix} \frac{J_\rho}{K_f L_h} & 0 \end{bmatrix} \nu_{2_{eq}} \,. \tag{28}$$

The right-hand side of the equation above can be computed on-line since it only depends on the output estimation error e_{y_2}. It is possible to compute $\nu_{2_{eq}}$ by filtering the discontinuous term ν_2 in (27) and then to detect the fault f_d.

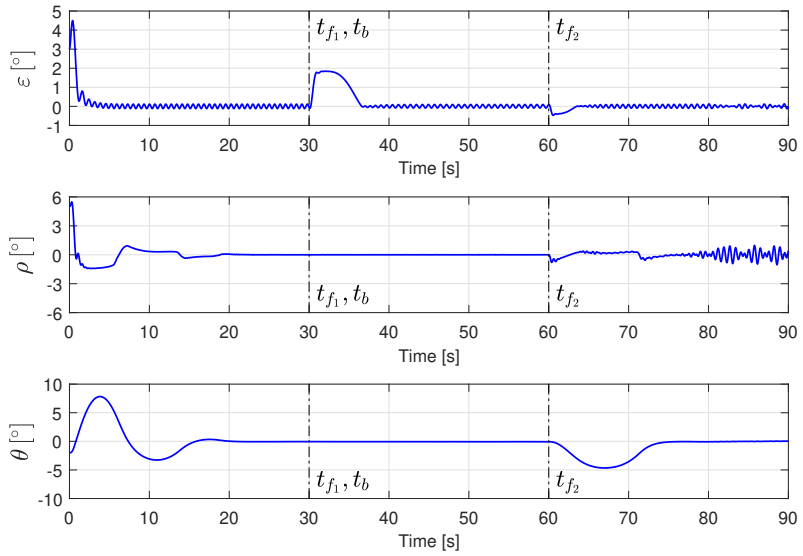

Figure 6: Angular positions of the 3-DoF helicopter prototype with the observers (22) and (26): simulation results.

6.3. Isolation of faults with the observer FDI procedure

Once the unknown input observers are able to detect the faults, this information can be used to isolate the faults, i.e. to know which one of the two motors is under failure conditions and at what time, even if the faults occur at the same time. In a similar way as presented in Section 4, the residual equations that allow detecting and isolating the presence of faults in any of the motors are in this case

$$R_f = f_s + f_d\,, \tag{29a}$$

$$R_b = f_s - f_d\,, \tag{29b}$$

for the front motor (29a) and for the back motor (29b).

6.4. Simulation results

The same conditions of simulation as in Section 5 are considered, both for initial conditions and for the gains of CTA controllers (10) and (14), respectively. Observer (22) was developed with parameters $\bar{A}^s_{22} = -10 \Rightarrow P_1 = 0.05$ and

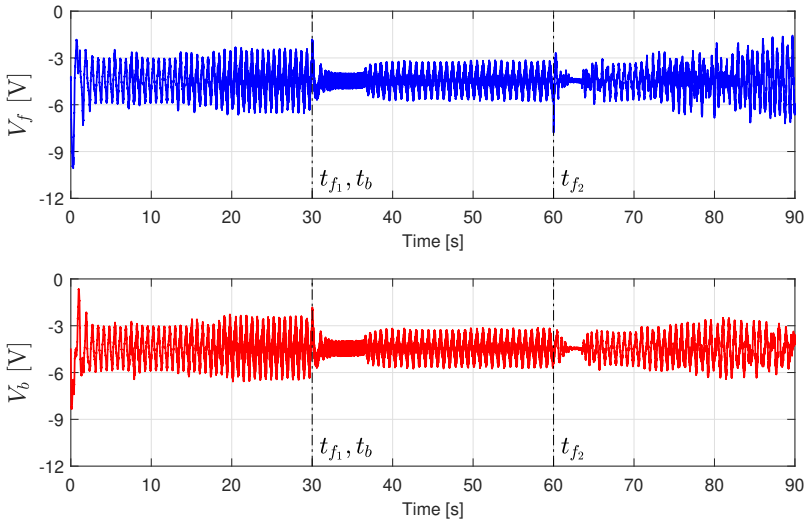

Figure 7: Voltage in motors with the observers (22) and (26): simulation results.

$\rho_1 = 20$. Observer (26) was developed with $\bar{A}^s_{22} = \text{diag}\{-10, -12\} \Rightarrow P_2 = \text{diag}\{0.05, 0.0417\}$, $\rho_{21} = 20$ and $\rho_{22} = 2$. Fig. 6 shows the angular positions of the 3-DoF helicopter prototype, it can be seen that combination of unknown inputs observers and CTA controllers are able to drive the trajectories to a vicinity of the origin even in presence of faults. The voltage of the motors that mitigate consequences of faults in the actuators of a 3-DoF helicopter prototype are plotted in Fig. 7. The residuals (24) and (28) are shown in Fig. 8. In addition, linear filters are used to construct the unknown inputs (24) and (28),

$$\mu_f \dot{\bar{f}}_s + \bar{f}_s = f_s \quad \text{and} \quad \mu_f \dot{\bar{f}}_d + \bar{f}_d = f_d \,. \tag{30}$$

with constant $\mu_f = 0.001$. An intermittent fault in the front motor of duration $T = t_{f_2} - t_{f_1} = 30$ seconds is detected by the residual (29a). A persistent fault in the back motor is detected by the residual (29b) from time $t_b = 30$ seconds, until the end of the simulation. Nevertheless, the observer-based FDI scheme is "vulnerable" to the lack of knowledge of K_f parameter, for example, which variation causes steady-state error in the angles of the 3-DoF helicopter prototype.

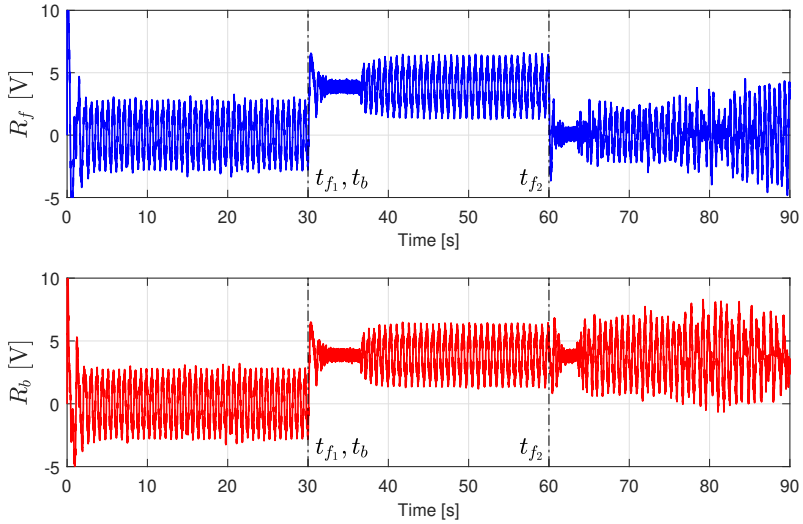

Figure 8: FDI signals (18a) and (18b) measured from the experimental setup with the observers (22) and (26): simulation results.

6.5. Comparison of Real-Time Implementability

Computational effort of the proposed controller is verified by the use of the *tic/toc* command in Matlab. The *tic* starts a stopwatch timer to measure performance, the function records the internal time at execution of the *tic* command. The computational effort of controllers can be validated analyzing the related Elapsed Real Time (ERT) exploiting the Real-Time Pacer MATLAB/Simulink Toolbox, which measures the real time elapsed to implement the algorithms. The elapsed time computation includes the nonlinear model in closed-loop with the fault tolerant controller and the FDI scheme based on differentiators or based on observers, respectively. Twenty simulations of each procedure are performed for the evaluation of the computational cost. The simulations were performed with AMD A6-1450 CPU @1.00 GHz Processor. A fixed sample frequency of 1000 Hz, with *ode1* Solver. Fig. 9 shows the ERT with expected differences on the order of 1-1.3 seconds from the reference value, i.e. 100 seconds, it means that both control schemes provide (quasi) *real-time* performance. The computational effort required to implement the CTA controllers based on differentiator

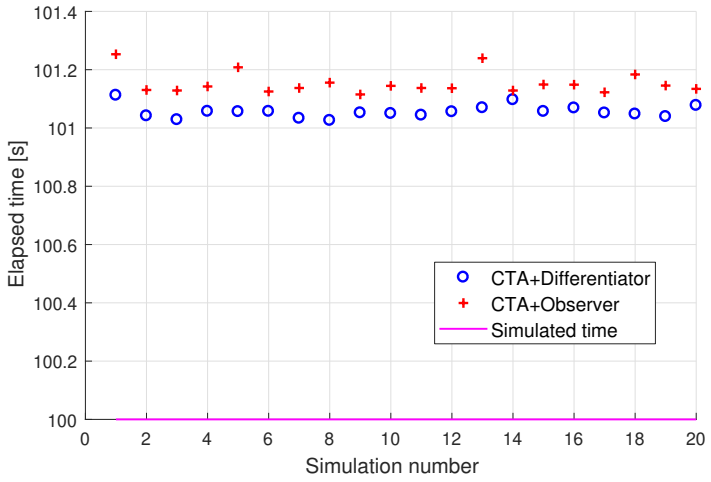

Figure 9: Elapsed Time for CTA algorithm with differentiator (proposed scheme) and with observer.

is almost the same as it is required for CTA controllers based on observer.

6.6. Analysis of comparison results

1. The observer based approach needs two extra sensors (physical or by software) to measure the velocities around the elevation and pitch axes, in order to satisfy relative degree condition, i.e. $\text{rank}(CB) = 1$, to construct the observers.

2. A combination of unknown inputs observers and CTA controllers mitigate the consequences of faults in the motors of the 3-DoF helicopter prototype. Nevertheless, the lack of knowledge of any parameter in the model, eg. K_f parameter, cause deviations respect to zero in the states of the closed-loop system response (see Fig. 11). The proposed methodology is robust with respect to parametric uncertainties (see Fig. 10), only the residuals need to be tuned in order to avoid a false detection of faults (see Fig. 5). For this reason, we use differentiators instead of observers, in which the exact model of the system is not needed.

3. The residual-based equations allow to detect and to isolate faults in the

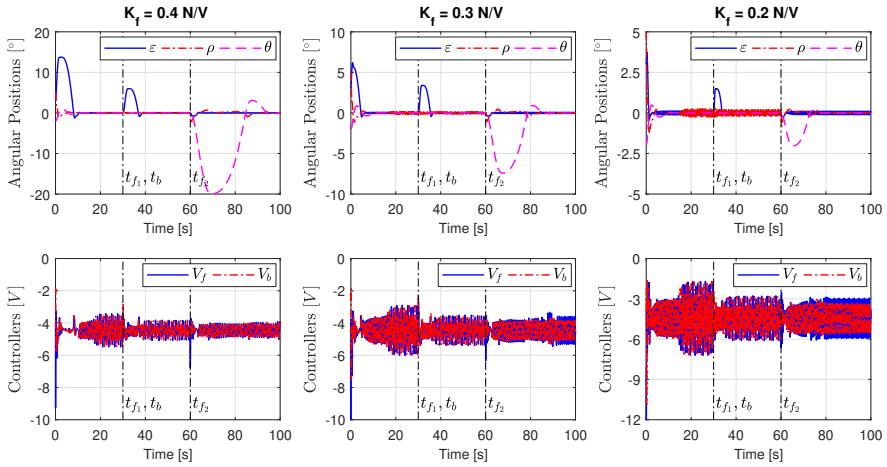

Figure 10: Angular positions and control inputs in presence of parametric uncertainties with CTA-based controllers and differentiator.

motors of the 3-DoF helicopter prototype, even if they occur at the same time.

4. Some oscillations (chattering) close to the origin should be caused by the presence of unmodeled dynamics (due to the actuator dynamics). However, the observer based approach causes fast oscillations of lower amplitude than those one caused by the differentiator based scheme.

5. The noise in the measurements strongly affects the residual detectors (18a)-(18b) as can be seen in Fig. 8. However, filtering of such residuals through (30) mitigate the consequences of the noise.

6. The computational effort required to implement the CTA controllers based on differentiator is almost the same as required for the classical observer based strategy, which makes the proposed algorithm suitable to be implemented.

7. Experimental Results

The 3-DoF helicopter prototype developed by Quanser is shown in Fig. 12. It is instrumented by three quadrature encoders with resolution 4096 pulse/rev

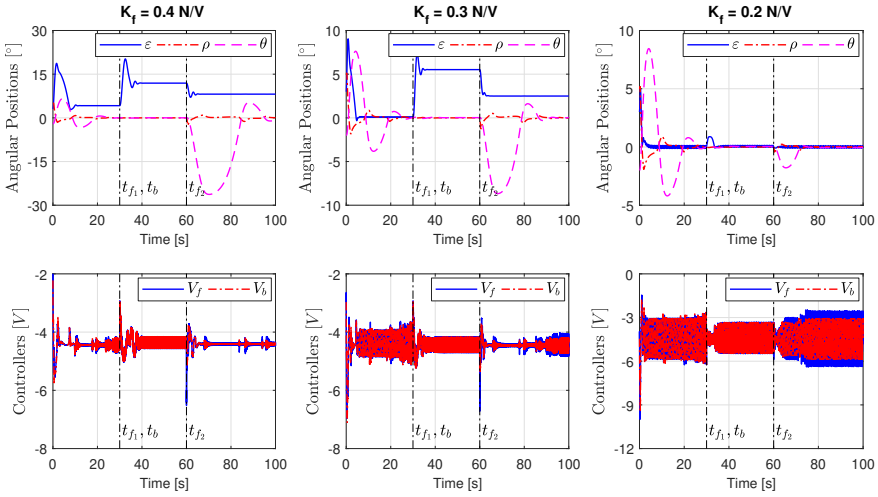

Figure 11: Angular positions and control inputs in presence of parametric uncertainties with CTA-based controllers and robust observer.

for the measurements of elevation ε and pitch ρ angles, and 8192 pulse/rev for the travel angle θ. The actuation system is composed by a pair of DC-motors (Pittman 9234S004 series). Measurements and signal processing are done by using a DSpace 1103 controller board composed by a high-speed Digital Signal Processor (DSP) PPC750GX of Texas Instruments developer. The Simulink scheme is exported to the EPROM memory of the board in which the Euler's integration method was used to solve the dynamical system of differentiator with fixed step $\tau = 10^{-4}$ seconds. The 3-DoF helicopter system is moved from the "home" position and the CTA controllers are activated to stabilize the system. The faults are induced by software after the settling time: an intermittent fault is forced in the front motor at time $t_{f_1} = 30$ seconds which stops at time $t_{f_2} = 60$ seconds. On the back motor a persistent fault appears at time $t_b = 30$ seconds and it remains throughout the experiment time. In both cases, 30% of drop voltage due to the faults is considered, i.e. $\gamma_f = \gamma_b = 0.7$.

The gains of the controller (10) are chosen $k_{11} = 4$, $k_{12} = 14$, $k_{13} = 0.2$, $k_{14} = 0$. On the other hand, the gains of the controller (14) are selected $k_{21} = 10$, $k_{22} = 14$, $k_{23} = 28$, $k_{24} = 0.2$, $k_{25} = 0$ and $k_{26} = 0$. The parameter of the sliding

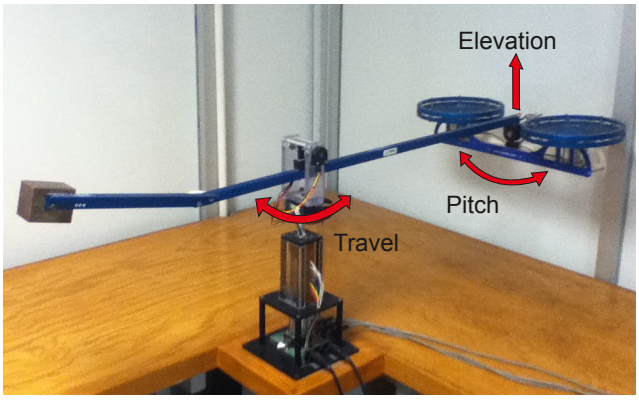

Figure 12: 3-DoF Helicopter Experimental Prototype

variable is fixed $c = 0.5$. The scaling parameters of the 3rd-order differentiator (19) are fixed $L_\varepsilon, L_\rho, L_\theta = 300$ as in simulations. Fig. 13 shows the angular positions of the 3-DoF helicopter prototype. It can be seen that CTA controllers are able to drive the trajectories to a vicinity of the origin, even in presence of faults. The voltage of the motors, that mitigate the consequences of faults, are in Fig. 14. The residual based equations of the front (18a) and the back (18b) motors are shown in Fig. 15. Although the effect of the faults can be appreciated, we opted to apply (online) first-order filters of the form

$$\mu_F \dot{\bar{R}}_f + \bar{R}_f = R_f \quad \text{and} \quad \mu_F \dot{\bar{R}}_b + \bar{R}_b = R_b \,. \tag{31}$$

The filtered residual-based equations are in Fig. 16, in which the presence of an intermittent fault in the front motor of duration $T = t_{f_2} - t_{f_1} = 30$ seconds. A persistent fault in the back motor from the time $t_b = 30$ seconds can be clearly seen. The parameter of the filters is $\mu_F = 0.2$.

7.1. Thresholds Adjustment

Figure 17 shows the residual-based equations (18a)-(18b) obtained by experiments: (left) $K_f = 0.4$ N/V; (center) $K_f = 0.3$ N/V; (right) $K_f = 0.2$ N/V. The residual equations (18a)-(18b) are mounted on offset levels due to lack of knowledge of K_f parameter (see residual offsets in Fig. 17 at left and center),

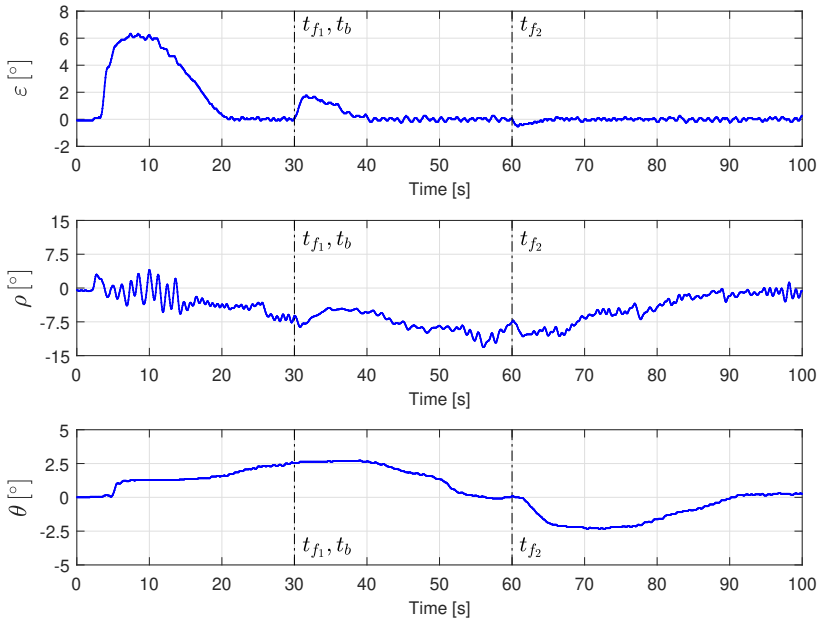

Figure 13: Angular positions of the 3-DoF helicopter prototype with CTA control laws (10)-(14): experimental results.

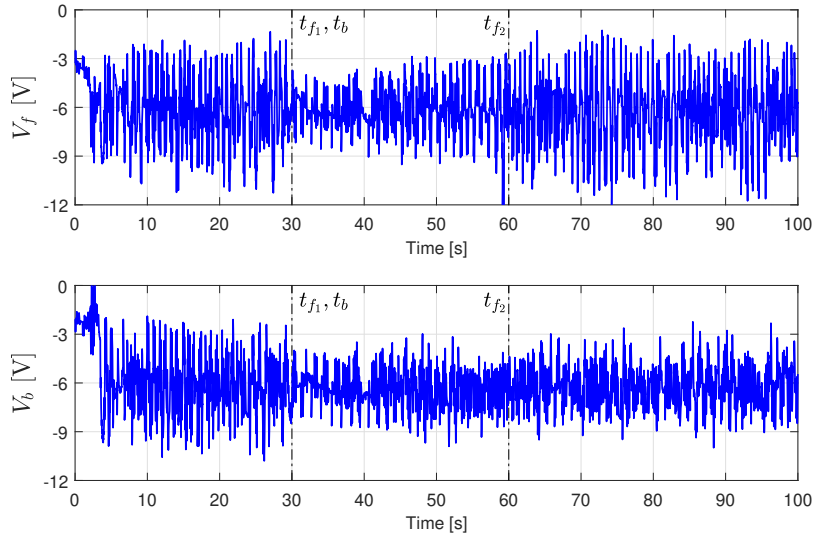

Figure 14: Voltage in motors with CTA control law: experimental results.

which imply false-positives in the FDI procedure. However, it is possible to adjust these offsets by tuning the K_f parameter (there are no residual offsets

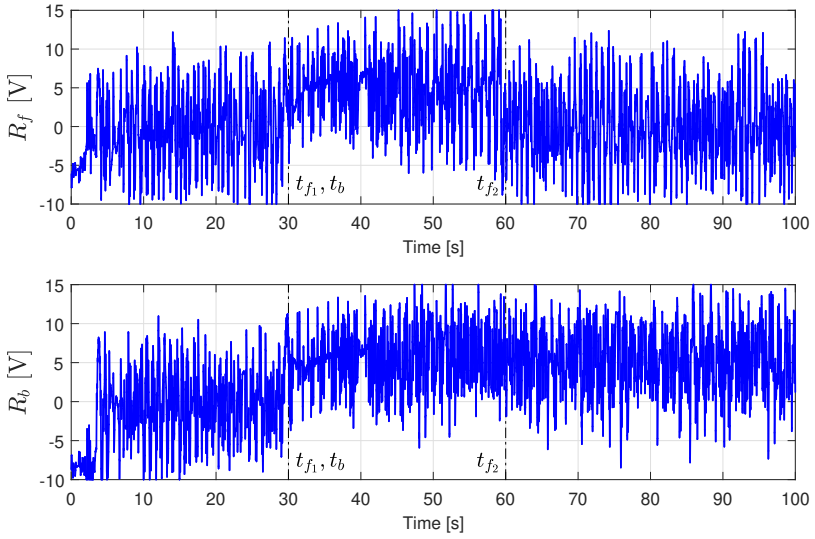

Figure 15: FDI signals (18a) and (18b) measured from the experimental setup with CTA control laws (10)-(14): experimental results.

in Fig. 17 at right). Note that proposed FDI scheme allows to determine the K_f parameter by experiments, provided that the controller is able to drive the system trajectories to a vicinity of the origin.

7.2. Analysis of experimental results

- The controllers based on CTA drive the trajectories to zero even in presence of faults, modeled as (2)-(3), in the motors of the 3-DoF helicopter prototype.
- The effects of noises and parasitic dynamics (actuators) strongly affect the FDI procedure. However, the faults can be clearly seen by filtering the residuals such as (31).
- The offset levels in the residual equations (18a)-(18b) can be mitigated by tuning the K_f parameter in the model (1a)-(1b)-(1c).
- The usege of accelerometers in Unmanned Aerial Vehicles (UAVs) is common. Then, it is feasible to implement FDI schemes based on residual

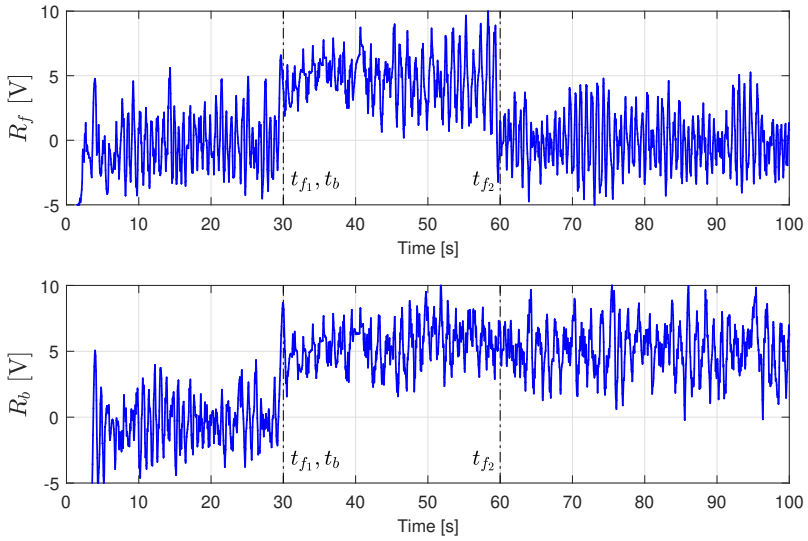

Figure 16: Filtered FDI signals (31) of the front (18a) and back (18b) motors with CTA control law: experimental results.

equations with the information of the accelerations following the ideas proposed in this paper.

8. Conclusions

In this paper, controllers based on the sliding mode Continuous Twisting Algorithm (CTA) are developed to steer the trajectories of a 3-DoF helicopter prototype to the origin, by means of continuous control signals. A fault detection and isolation scheme is provided through residual-based equations, that require the availability of the system accelerations. In order to propose a *sensorless* procedure, third-order sliding mode differentiators are used not only to obtain the accelerations, but also to know the state (the helicopter velocities), starting from the angular positions of the helicopter. A comparison with respect to a classic observer-based FDI procedure is given to highlight the advantages of the proposed method. Simulations and experimental results show that CTA-based controllers can be used for tolerance of matched faults, ensuring robust stabilization of the equilibrium point, using a simplest model of

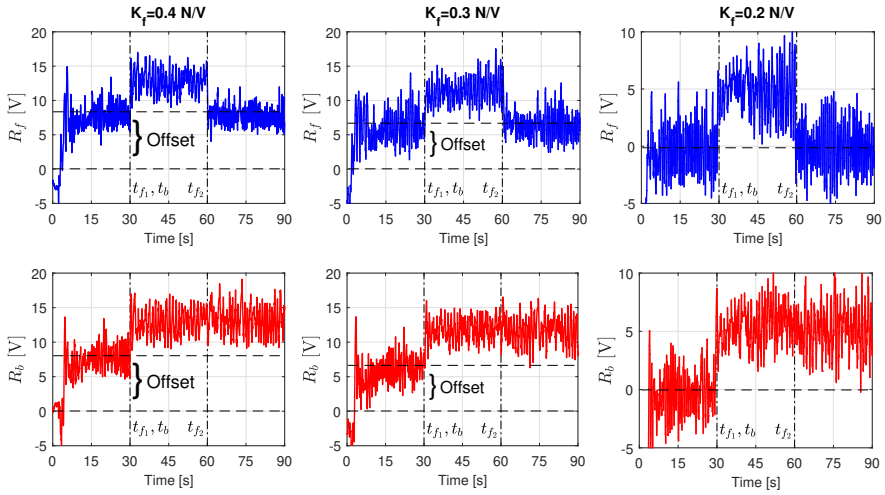

Figure 17: Tuning of thresholds for residual-based detection and isolation of faults: experimental results.

the helicopter dynamics and the information of angular positions and velocities. The differentiator-based FDI method shows better performance compared to the observer-based FDI method, in presence of parametric uncertainties in the model. Filtering signals obtained by residual equations is suggested in order to mitigate the effects of noises and fast-parasitic dynamics on the FDI procedure.

Appendix

Proposition 1 is based on the equivalent control concept [35]. Note that at the equilibrium point $X = [\bar{\varepsilon}, 0, \bar{\theta}, 0, 0, 0]^\top$, the control inputs are

$$u_{s_{eq}} = -\frac{\tau_g \cos(\bar{\varepsilon})}{K_f L_a}, \quad u_{d_{eq}} = 0,$$

which implies the motor voltages

$$V_{f_{eq}} = V_{b_{eq}} = -\frac{\tau_g \cos(\bar{\varepsilon})}{2K_f L_a}. \tag{32}$$

8.1. Detection of Faults in the Front Motor

When a fault occurs in the front motor, the elevation dynamics (1a) is such that

$$\ddot{\varepsilon} = \frac{K_f L_a}{J_\varepsilon} \cos(\rho)\big(\gamma_f V_f + V_b\big) + \frac{\tau_g \cos(\varepsilon)}{J_\varepsilon}.$$

On the other hand, the pitch dynamics (1b) is

$$\ddot{\rho} = \frac{K_f L_h}{J_\rho}\big(\gamma_f V_f - V_b\big)\,.$$

After a transient time, the sliding-mode controller compensates theoretically exactly the fault and the trajectories reach the equilibrium point X. Then, the control inputs are

$$u_{s_{eq}} = -\left(1 + \frac{1}{\gamma_f}\right)\frac{\tau_g \cos(\bar{\varepsilon})}{2K_f L_a}\,, \tag{33a}$$

$$u_{d_{eq}} = \quad \left(1 - \frac{1}{\gamma_f}\right)\frac{\tau_g \cos(\bar{\varepsilon})}{2K_f L_a}\,, \tag{33b}$$

by substituting the control inputs (33a) and (33b) into the residual states (17a) and (17b), respectively,

$$R_{\varepsilon_{eq}} = -\left(1 - \frac{1}{\gamma_f}\right)\frac{\tau_g \cos(\bar{\varepsilon})}{2K_f L_a}\,,$$

$$R_{\rho_{eq}} = -\left(1 - \frac{1}{\gamma_f}\right)\frac{\tau_g \cos(\bar{\varepsilon})}{2K_f L_a}\,.$$

Finally, the motor voltages (32) are obtained as reported in Table 3 (column 2).

8.2. Detection of Faults in the Back Motor

In a similar way, when a fault occurs in the back motor, the elevation dynamics (1a) is such that

$$\ddot{\varepsilon} = \frac{K_f L_a}{J_\varepsilon}\cos(\rho)\big(V_f + \gamma_b V_b\big) + \frac{\tau_g \cos(\varepsilon)}{J_\varepsilon}\,,$$

and the pitch dynamics (1b) is

$$\ddot{\rho} = \frac{K_f L_h}{J_\rho}\big(V_f - \gamma_b V_b\big)\,.$$

After a transient time, the sliding-mode controller compensates theoretically exactly the fault and the control inputs are of form

$$u_{s_{eq}} = -\left(1 + \frac{1}{\gamma_b}\right)\frac{\tau_g \cos(\bar{\varepsilon})}{2K_f L_a}\,, \tag{35a}$$

$$u_{d_{eq}} = -\left(1 - \frac{1}{\gamma_b}\right)\frac{\tau_g \cos(\bar{\varepsilon})}{2K_f L_a}\,, \tag{35b}$$

by substituting the control inputs (35a) and (35b) into the residual states (17a) and (17b), respectively,

$$R_{\varepsilon_{eq}} = -\left(1 - \frac{1}{\gamma_b}\right) \frac{\tau_g \cos(\bar{\varepsilon})}{2K_f L_a},$$
$$R_{\rho_{eq}} = \left(1 - \frac{1}{\gamma_b}\right) \frac{\tau_g \cos(\bar{\varepsilon})}{2K_f L_a}.$$

Finally, the motor voltages (32) are obtained as reported in Table 3 (column 3).

8.3. Detection of Simultaneous Faults

When faults occur in both motors, the elevation dynamics (1a) is such that

$$\ddot{\varepsilon} = \frac{K_f L_a}{J_\varepsilon} \cos(\rho)\big(\gamma_f V_f + \gamma_b V_b\big) + \frac{\tau_g \cos(\varepsilon)}{J_\varepsilon},$$

and the pitch dynamics (1b) is

$$\ddot{\rho} = \frac{K_f L_h}{J_\rho}\big(\gamma_f V_f - \gamma_b V_b\big),$$

After a transient time, the sliding-mode controller compensates theoretically exactly the fault and the control inputs are of form

$$u_{s_{eq}} = -\left(\frac{\gamma_f + \gamma_b}{\gamma_f \gamma_b}\right) \frac{\tau_g \cos(\bar{\varepsilon})}{2K_f L_a}, \tag{37a}$$
$$u_{d_{eq}} = \left(\frac{\gamma_f - \gamma_b}{\gamma_f \gamma_b}\right) \frac{\tau_g \cos(\bar{\varepsilon})}{2K_f L_a}, \tag{37b}$$

then by substituting the control inputs (37a) and (37b) into the residual states (17a) and (17b), respectively,

$$R_{\varepsilon_{eq}} = -\left(2 - \frac{\gamma_f + \gamma_b}{\gamma_f \gamma_b}\right) \frac{\tau_g \cos(\bar{\varepsilon})}{2K_f L_a}, \tag{38a}$$
$$R_{\rho_{eq}} = -\left(\frac{\gamma_f - \gamma_b}{\gamma_f \gamma_b}\right) \frac{\tau_g \cos(\bar{\varepsilon})}{2K_f L_a}. \tag{38b}$$

Finally, the motor voltages (32) are obtained as reported in Table 3 (column 4).

Remark 3. *The fault detection and isolation scheme is based on the fact that the voltages V_f and V_b are not zero at any time. This effect is mainly due to the gravitational torque $\tau_g = g(M_h L_a - M_w L_w)$ around the elevation axis.*

Remark 4. *In presence of simultaneous faults of the same magnitude, i.e.* $\gamma_f = \gamma_b$*, the logical state (17b) related to the pitch dynamics will be zero (see expression (38b)), which means that faults are hidden. However the logical state (17a) related to the elevation dynamics will be different from zero, which allows to isolate the faults.*

ACKNOWLEDGMENT

The authors are grateful for the financial support of CONACyT (Consejo Nacional de Ciencia y Tecnología): CVU 631266; Project 282013; PAPIIT-UNAM (Programa de Apoyo a Proyectos de Investigación e Innovación Tecnológica): IN 115419; PASPA-UNAM (Programa de Apoyos para la Superación del Personal Académico de la UNAM); Bilateral cooperation Italy-Mexico 234791.

9. References

[1] J. Apkarian, M. Lvis, C. Fulford, Laboratory Guide 3 DOF Helicopter Experiment for MATLAB/Simulink Users 1st ed., Markham, Ontario, Canada: Quanser Inc., 2012.
URL `https://www.quanser.com/products/3-dof-helicopter/`

[2] V. Utkin, Sliding modes in optimization and control problems, Springer Verlag, New York, 1992.

[3] K. K. Starkov, L. T. Aguilar, Y. Orlov, Sliding mode control synthesis of a 3-dof helicopter prototype using position feedback, in: 2008 IEEE International Workshop on Variable Structure Systems (VSS), IEEE, 2008, pp. 233–237.

[4] H. Ríos, A. Rosales, A. Dávila, Global non-homogeneous quasi-continuous controller for a 3-dof helicopter, in: 2010 11th International Workshop on Variable Structure Systems (VSS), IEEE, 2010, pp. 475–480.

[5] I. M. Meza-Sánchez, Y. Orlov, L. T. Aguilar, Stabilization of a 3-dof underactuated helicopter prototype: Second order sliding mode algorithm synthesis, stability analysis, and numerical verification, in: 2012 12th International Workshop on Variable Structure Systems (VSS), IEEE, 2012, pp. 361–366.

[6] F. Plestan, A. Chriette, A robust controller based on adaptive supertwisting algorithm for a 3dof helicopter, in: 2012 IEEE 51st Annual Conference on Decision and Control (CDC), IEEE, 2012, pp. 7095–7100.

[7] U. Pérez-Ventura, L. Fridman, When is it reasonable to implement the discontinuous sliding-mode controllers instead of the continuous ones? frequency domain criteria, International Journal of Robust and Nonlinear Control (2018) 810–828.
URL DOI:10.1002/rnc.4347

[8] A. Ferreira de Loza, H. Ríos, A. Rosales, Robust regulation for a 3-dof helicopter via sliding-mode observation and identification, Journal of the Kranklin Institute 349 (2) (2012) 700–718.

[9] E. Vázquez, U. P. Ventura, D. Hernández, Continuous sliding-mode controllers for a 3-dof helicopter, in: 2017 14th International Conference on Electrical Engineering, Computing Science and Automatic Control (CCE), IEEE, 2017, pp. 1–6.

[10] L. Fridman, J. A. Moreno, B. Bandyopadhyay, S. Kamal, A. Chalanga, Continuous nested algorithms: The fifth generation of sliding mode controllers, Recent Advances in Sliding Modes: From Control to Intelligent Mechatronics 24 (2015) 5–35.

[11] X. Qi, D. Theilliol, J. Qi, Y. Zhang, J. Han, A literature review on fault diagnosis methods for manned and unmanned helicopters, in: 2013 International Conference on Unmanned Aircraft Systems (ICUAS), IEEE, 2013, pp. 1114–1118.

[12] J. C. da Silva, A. Saxena, E. Balaban, K. Goebel, A knowledge-based system approach for sensor fault modeling, detection and mitigation, Expert Systems with Applications 39 (12) (2012) 10977–10989.

[13] D. Yang, Y. Ren, Z. Wang, L. Liu, B. Sun, A novel logic-based approach for failure modes mitigation control and quantitative system reliability analyses, Eksploatacja i Niezawodność 17.

[14] R. Isermann, Process fault detection based on modeling and estimation methodsa survey, Automatica 20 (4) (1984) 387–404.

[15] R. Isermann, Model-based fault detection and diagnosis-status and applications, IFAC Proceedings Volumes 37 (6) (2004) 49–60.

[16] J. Chen, R. J. Patton, Robust model-based fault diagnosis for dynamic systems, Vol. 3, Springer Science & Business Media, 2012.

[17] A. Zolghadri, The challenge of advanced model-based fdir for real-world flight-critical applications, Engineering Applications of Artificial Intelligence 68 (2018) 249–259.

[18] M. Bartyś, Generalized reasoning about faults based on the diagnostic matrix, International Journal of Applied Mathematics and Computer Science 23 (2) (2013) 407–417.

[19] J. Korbicz, J. M. Koscielny, Z. Kowalczuk, W. Cholewa, Fault Diagnosis: Models, Artificial Intelligence, Applications, Springer Science & Business Media, 2004.

[20] H. An, J. Liu, C. Wang, L. Wu, Approximate back-stepping fault-tolerant control of the flexible air-breathing hypersonic vehicle, IEEE/ASME Transactions on Mechatronics 21 (3) (2015) 1680–1691.

[21] M. Zhang, P. Shi, C. Shen, Z.-G. Wu, Static output feedback control of switched nonlinear systems with actuator faults, IEEE Transactions on Fuzzy Systems.

[22] Y. Zhao, J. Wang, F. Yan, Y. Shen, Adaptive sliding mode fault-tolerant control for type-2 fuzzy systems with distributed delays, Information Sciences 473 (2019) 227–238.

[23] J. Marzat, H. Piet-Lahanier, F. Damongeot, E. Walter, Model-based fault diagnosis for aerospace systems: a survey, Proceedings of the Institution of Mechanical Engineers, Part G: Journal of aerospace engineering 226 (10) (2012) 1329–1360.

[24] C. Edwards, H. Alwi, C. Tan, Sliding mode methods for fault detection and fault tolerant control with application to aerospace systems, International Journal of Applied Mathematics and Computer Science 22 (1) (2012) 109–124.

[25] C. Edwards, S. K. Spurgeon, R. J. Patton, Sliding mode observers for fault detection and isolation, Automatica 36 (4) (2000) 541–553.

[26] W. Chen, M. Saif, Actuator fault diagnosis for uncertain linear systems using a high-order sliding-mode robust differentiator (hosmrd), International Journal of Robust and Nonlinear Control 18 (4-5) (2008) 413–426.

[27] H. Mekki, O. Benzineb, D. Boukhetala, M. Tadjine, M. Benbouzid, Sliding mode based fault detection, reconstruction and fault tolerant control scheme for motor systems, ISA transactions 57 (2015) 340–351.

[28] H. Ríos, C. Edwards, J. Davila, L. Fridman, Fault detection and isolation for nonlinear systems via high-order-sliding-mode multiple-observer, International Journal of Robust and Nonlinear Control 25 (16) (2015) 2871–2893.

[29] H. Ríos, E. Punta, L. Fridman, Fault detection and isolation for nonlinear non-affine uncertain systems via sliding-mode techniques, International Journal of Control 90 (2) (2017) 218–230.

[30] E. Capello, E. Punta, L. Fridman, Strategies for control, fault detection and isolation via sliding mode techniques for a 3-dof helicopter, in: 2016

IEEE 55th Conference on Decision and Control (CDC), IEEE, 2016, pp. 6464–6469.

[31] A. Levant, Higher-order sliding modes, differentiation and output-feedback control, International journal of Control 76 (9-10) (2003) 924–941.

[32] V. Torres-González, T. Sanchez, L. M. Fridman, J. A. Moreno, Design of continuous twisting algorithm, Automatica 80 (2017) 119–126.

[33] U. P. Ventura, E. Capello, E. Punta, , J. Perea, L. Fridman, Fault detection and isolation for a 3-dof helicopter with sliding mode strategies, in: 2018 15th International Workshop on Variable Structure Systems (VSS), IEEE, Graz, Austria, 2018, pp. 279–284.

[34] J. Mendoza-Avila, J. A. Moreno, L. Fridman, Continuous twisting algorithm for third order systems, IEEE Transactions on Automatic Control (2019) 1–12.
URL DOI:10.1109/TAC.2019.2932690

[35] Y. Shtessel, C. Edwards, L. Fridman, A. Levant, Sliding mode control and observation, Birkhäuser, Boston, 2014.

[36] M. A. Golkani, L. M. Fridman, S. Koch, M. Reichhartinger, M. Horn, Saturated continuous twisting algorithm, in: 2018 15th International Workshop on Variable Structure Systems (VSS), IEEE, 2018, pp. 138–143.

[37] M. A. Golkani, S. Koch, M. Reichhartinger, M. Horn, L. Fridman, Saturated feedback control using different higher-order sliding-mode algorithms, in: Variable-Structure Systems and Sliding-Mode Control, Springer, 2020, pp. 125–148.

[38] R. Seeber, M. Reichhartinger, Conditioned super-twisting algorithm for systems with saturated control action, Automatica.

[39] C. Edwards, S. K. Spurgeon, On the development of discontinuous observers, International Journal of control 59 (5) (1994) 1211–1229.